Available online at www.sciencedirect.com

ScienceDirect

Focus Article, *Mendeleev Commun.*, 2024, **34**, 307–315

Mendeleev Communications

Electronic structures of transition metal sandwich complexes revisited by high-resolution laser spectroscopy coupled with DFT

Sergey Yu. Ketkov

G. A. Razuvaev Institute of Organometallic Chemistry, Russian Academy of Sciences, 603950 Nizhny Novgorod, Russian Federation. E-mail: sketkov@iomc.ras.ru

DOI: 10.1016/j.mencom.2024.04.002

Laser photoionization spectroscopy provides extremely high accuracy in determining ionization energies of jet-cooled bisarene complexes, metallocenes and mixed sandwich compounds as well as vibrational frequencies of free sandwich ions. Combined with DFT calculations, these experimental data give unique information on the structure–property relationships in sandwich molecules. New aspects of fine substituent effects as well as structural transformations of sandwich complexes on ionization are discussed.

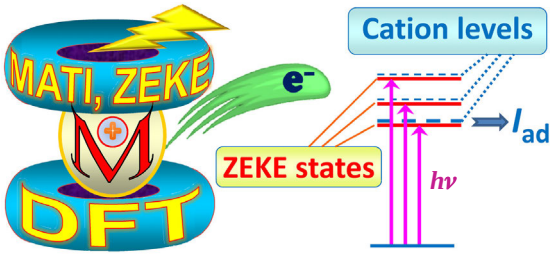

Keywords: transition metals, sandwich compounds, laser ionization spectroscopy, DFT calculations, electronic structure, ionization energy.

Introduction

The discovery of the unique sandwich structures of ferrocene[1,2] and bis(η^6-benzene)chromium[3] in the 1950s opened the door to a new era of organometallic chemistry. Advances and breakthroughs in this field led to the Nobel prize in chemistry awarded half a century ago to E. O. Fischer and G. Wilkinson 'for their pioneering work, performed independently, on the chemistry of the organometallic, so called sandwich compounds'.[4] In recent decades, increased interest in sandwich systems has been due to their relevance for the theory of bonding in metal complexes,[5–8] chemistry of metallopolymers,[9–13] electrochemistry,[14–17] catalysis,[18–20] nanoelectronics[21–27] and biomedicine.[28–32]

Metallocenes and related compounds possess very low ionization energies (5–7 eV).[33–36] Their ability to form stable or reactive molecular ions plays an essential role in many areas of practical use including medicine,[30–32] sensors,[37–39] batteries[40,41] and molecular electronics.[24–26,42] Therefore, the ionization parameters of sandwich molecules as well as the transformations of molecular and electronic structures accompanying the electron detachment deserve thorough study. Unprecedented opportunities for such investigations are provided by zero kinetic energy (ZEKE) and mass-analyzed threshold ionization (MATI) laser spectroscopies.[43,44] In these techniques, jet-cooled neutrals are excited by laser irradiation to long-lived high Rydberg states (so called ZEKE states) and then ionized by a delayed electrical pulse. ZEKE and MATI methods provide extremely high accuracy in determination of ionization energies of neutral molecules and vibrational frequencies of free ions. This information unveils new details of molecular and electronic structures of various compounds.

High-resolution experimental molecular parameters obtained from ZEKE/MATI spectra form a unique basis for validating quantum chemical calculations. In turn, computational chemistry provides insight into the intramolecular interactions responsible for the features revealed by laser spectroscopy. Therefore, a combination of ZEKE/MATI experiments with DFT calculations represents a powerful instrument for studying molecular systems. However, the use of ZEKE/MATI spectroscopy to study metal complexes is extremely challenging due to their thermal and chemical instability. Nevertheless, over the past two decades, promising results have been obtained on some bisarene complexes, metallocenes, and heteroligand sandwich compounds. A brief overview of these achievements is presented in this article.

Ionization energies of sandwich neutrals and vibrational frequencies of ions

Most ZEKE/MATI studies of sandwich molecules deal with bisarene complexes (Table 1). The ionized orbital in the complexes of Group 6 metals is non-bonding MO a_1 that represents an almost 'pure' metal d_{z^2} wavefunction. Accordingly,

Sergey Ketkov is Head of a Laboratory of the Structure of Organometallic and Coordination Compounds at the G. A. Razuvaev Institute of Organometallic Chemistry RAS (Nizhny Novgorod). His research interests include electronic structures, reactivity and spectroscopic properties of metal complexes studied with various experimental and theoretical approaches. He published more than 180 peer-reviewed research articles in Russian and international scientific journals.

Table 1 High-resolution adiabatic ionization energies I_{ad} (cm^{-1}) of neutral sandwich compounds and the frequencies of the metal–ligand symmetric stretching mode in free sandwich cations determined by the ZEKE and MATI methods. The I_{ad} accuracy is given in parentheses.

Compound	I_{ad}	ν_{M-L}	Method	Reference
Bisarene complexes				
$(\eta^6\text{-}C_6H_6)_2Ti$	46231(8)	228	ZEKE	45
$(\eta^6\text{-}C_6H_6)_2V$	46651(16)	230	ZEKE	45
$(\eta^6\text{-}C_6H_6)_2Cr$	44087(5)	262	MATI	46
$(\eta^6\text{-}C_6H_6)_2Cr$	44087(5)	264	MATI	47
$(\eta^6\text{-}C_6H_6)_2Cr$	44090(3)	272	MATI	48
$(\eta^6\text{-}C_6H_6)_2Cr$	44081(5)	264	ZEKE	49
$(\eta^6\text{-}C_6H_6)_2Cr\cdot Ar$	43941(5)	262	MATI	47
$(\eta^6\text{-}C_6H_6)_2Cr\cdot C_6H_6$	42576(5)	271	MATI	47
$(\eta^6\text{-}C_6H_6)_2Mo$	44581(5)	277	ZEKE	49
$(\eta^6\text{-}C_6H_6)_2W$	43634(5)	370	ZEKE	49
$(\eta^6\text{-}C_6D_6)_2Cr$	44004(5)	249	MATI	50
$(\eta^6\text{-}C_6H_6)(\eta^6\text{-}C_6D_5H)Cr$	44007(5)	251	MATI	50
$(\eta^6\text{-}MeC_6H_5)(\eta^6\text{-}C_6H_6)Cr$	43392(5)	273	MATI	51
$(\eta^6\text{-}Ph_2)(\eta^6\text{-}C_6H_6)Cr$	43374(5)	273	MATI	51
$(\eta^6\text{-}1,3\text{-}Me_2C_6H_4)(\eta^6\text{-}C_6H_6)Cr$	42750(5)	283	MATI	52
$(\eta^6\text{-}MeC_6H_5)_2Cr^a$	42741(5)	262	ZEKE	53
$(\eta^6\text{-}MeC_6H_5)_2Cr^a$	42747(5)	268, 274	ZEKE	53
$(\eta^6\text{-}MeC_6H_5)_2Cr^a$	42746(5)	291	MATI	52
$(\eta^6\text{-}MeC_6H_5)_2Cr^b$	42807(5)	291	ZEKE	53
$(\eta^6\text{-}MeC_6H_5)_2Cr^b$	42809(5)	295	MATI	52
$(\eta^6\text{-}MeC_6H_5)_2Mo^a$	43440(5)	268	ZEKE	53
$(\eta^6\text{-}MeC_6H_5)_2Mo^a$	43448(5)	260	ZEKE	53
$(\eta^6\text{-}MeC_6H_5)_2Mo^b$	43522(5)	294	ZEKE	53
$(\eta^6\text{-}MeC_6H_5)_2W^a$	42567(5)	386	ZEKE	53
$(\eta^6\text{-}MeC_6H_5)_2W^b$	42655(5)	432	ZEKE	53
$(\eta^6\text{-}Ph_2)(\eta^6\text{-}MeC_6H_5)Cr$	42771(8)	280	MATI	54
$(\eta^6\text{-}Ph_2)_2Cr$	42812(8)	–	MATI	54
$(\eta^6\text{-}EtC_6H_5)_2Cr$	42379(5)	320	MATI	55
$(\eta^6\text{-}EtC_6H_5)_2Cr$	42463(5)	–	MATI	55
$(\eta^6\text{-}Pr^iC_6H_5)_2Cr$	42104(5)	–	MATI	55
$(\eta^6\text{-}Bu^tC_6H_5)_2Cr$	41917(5)	–	MATI	55
$(\eta^6\text{-}1,3,5\text{-}Me_3C_6H_3)_2Cr^a$	40357(5)	–	ZEKE	56
$(\eta^6\text{-}1,3,5\text{-}Me_3C_6H_3)_2Cr^b$	40559(5)	–	ZEKE	56
$(\eta^6\text{-}1,3,5\text{-}Me_3C_6H_3)_2Mo^b$	41697(5)	315	ZEKE	56
$(\eta^6\text{-}1,3,5\text{-}Me_3C_6H_3)_2W^b$	41000(5)	323	ZEKE	56
Metallocenes				
$(\eta^5\text{-}C_5Me_5)_2Mn$	43142(8)	340	MATI	57
$(\eta^5\text{-}C_5H_5)_2Co$	42969(5)	309	MATI	58
$(\eta^5\text{-}MeC_5H_4)(\eta^5\text{-}C_5H_5)Co$	42019(5)	312	MATI	59
Mixed sandwich compounds				
$(\eta^8\text{-}C_8H_8)(\eta^5\text{-}C_5H_5)Ti$	44464(5)	231	MATI	60
$(\eta^7\text{-}C_7H_7)(\eta^5\text{-}C_5H_5)Cr$	45243(5)	257	MATI	60

[a] The conformers with staggered Me groups. [b] The conformer with eclipsed Me groups.

the adiabatic and vertical ionization energies, I_{ad} and I_{vert}, coincide and correspond to the origin in the ZEKE or MATI spectra. The I_{ad} values are determined by these methods with an extremely high accuracy (usually ± 5 cm^{-1}, or ± 0.0006 eV). The parameters of individual bisarene complexes determined by different research groups using the ZEKE and MATI methods are in excellent mutual agreement (see Table 1).

The precise ionization parameters make it possible to study very weak influence of isotopic substitution on the electronic structure of $(\eta^6\text{-}C_6H_6)_2Cr$.[50] Even an extremely small difference of 3 cm^{-1} between I_{ad} of $(\eta^6\text{-}C_6D_6)_2Cr$ and $(\eta^6\text{-}C_6H_6)(\eta^6\text{-}C_6D_6H_5)Cr$ can be revealed (see Table 1) when measuring the threshold ionization spectra simultaneously in one MATI experiment. This difference is only 0.007% of the measured I_{ad} values. It can be shown[61] that the decrease in I_{ad} upon full deuteration of $(\eta^6\text{-}C_6H_6)_2Cr$ corresponds to the difference between the $(E_{ZPE}^{cation} - E_{ZPE}^{neutral})$ values in $(\eta^6\text{-}C_6H_6)_2Cr$ and $(\eta^6\text{-}C_6D_6)_2Cr$, where E_{ZPE}^{cation} and $E_{ZPE}^{neutral}$ are zero-point vibrational energies of the cation and neutral, respectively. Therefore, the accurate I_{ad} parameters of $(\eta^6\text{-}C_6H_6)_2Cr$ and $(\eta^6\text{-}C_6D_6)_2Cr$ also provide important experimental information on the relative E_{ZPE} values.

The high resolution of the MATI and ZEKE spectra opens up exceptional opportunities to study the effects of substituents in sandwich complexes. The spectra of Group 6 metal methylated benzene complexes appear to detect individual rotational isomers.[44,52,53,55,56] The benzene rings in bisarene complexes are eclipsed so the Me groups in the two ligands can be located at specific dihedral angles [0°, an eclipsed rotamer, and 60, 120 and 180°, staggered rotamers, for $(\eta^6\text{-}MePh)_2M$; 0 and 60 ° for $(\eta^6\text{-}1,3,5\text{-}Me_3C_6H_3)_2M$]. The corresponding neutral and cationic rotational isomers possess different electronic energies (Figure 1) and different I_{ad}. However, the difference in I_{ad} is too small to make the rotamers distinguishable by 'classical' photoelectron spectroscopy.[33] On the contrary, the MATI and ZEKE spectra show well-resolved origins corresponding to each rotational isomer (Figure 2). In the methylated systems, the ionization energies of the eclipsed rotamers (dihedral angle of 0°) appear to be higher than those of the complexes bearing staggered substituents (see Table 1).

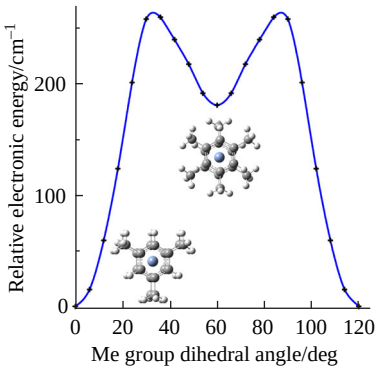

Figure 1 Electronic energy scan (the B3LYP functional) of $(\eta^6\text{-}1,3,5\text{-}Me_3C_6H_3)_2Cr$ as a function of methyl group dihedral angles. The structures correspond to the 0° and 60° rotational conformers. Reprinted with permission from ref. 56. Copyright 2013 American Chemical Society.

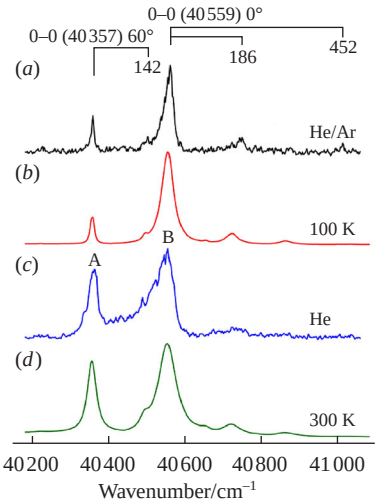

Figure 2 Experimental ZEKE spectra of $(\eta^6\text{-}1,3,5\text{-}Me_3C_6H_3)_2Cr$ seeded in the (*a*) 1:1 He/Ar and (*c*) He carrier gases and spectral simulations at (*b*) 100 and (*d*) 300 K. Reprinted with permission from ref. 56. Copyright 2013 American Chemical Society.

This effect is associated with the mutual influence of the Me groups.

To analyse the 'pure' influence of a substituent in a benzene ring of a bisarene system, the ionization energies of monosubstituted species are necessary. Such data are available for the methylated and phenylated chromium complexes.[51] The I_{ad} values of (η^6-toluene)(η^6-benzene)chromium and (η^6-biphenyl)(η^6-benzene)chromium are determined by the MATI method as 43392(5) and 43374(5) cm^{-1}, respectively (see Table 1). The ionization energy decreases by 695 and 713 cm^{-1} on the introduction of a single Me and Ph fragment, respectively, into a benzene ring of bis(η^6-benzene)chromium. Then the red shift of I_{ad}, caused by two Me groups not interacting with each other, is predicted to be 695 × 2 = 1390 cm^{-1}. The experimental decrease in I_{ad} when replacing two benzene ligands of (η^6-C_6H_6)$_2$Cr with toluene is smaller (1341 cm^{-1} for the staggered rotamers and 1280 cm^{-1} for the eclipsed complex). Therefore, the Me–Me interactions reduce the influence of the second Me substituent.

Comparison of the predicted I_{ad} of (η^6-MePh)$_2$Cr and the ZEKE/MATI data reveals two types of the Me–Me mutual influence (Figure 3). The experimental ionization energy of the staggered rotamers (the Me dihedral angle of 60, 120 and 180°) are 49 cm^{-1}, or 0.6 kJ mol^{-1}, larger than the predicted value. This difference corresponds to the Me–Me influence of Type 1.[51] For the eclipsed conformer, where a direct interaction between the Me groups in two rings becomes possible, an additional shift of 61 cm^{-1}, or 0.8 kJ mol^{-1} (Type 2 interaction) is observed (see Figure 3). The Type-2 energy E_2 exceeds slightly the Type-1 energy E_1 in (η^6-MeC_6H_5)$_2$Cr. The Type-1 Me–Me interactions involve the sandwich core. They are characteristic for any polymethylated bisarene system.[51] The I_{ad} values of the (η^6-MeC_6H_5)$_2$Cr staggered rotamers are very close to I_{ad} of (η^6-1,3-$Me_2C_6H_4$)(η^6-C_6H_6)Cr (see Table 1), which testifies for equal shifts caused by the intraligand and interligand Type-1 Me–Me influence. Being very low in bis(η^6-toluene)chromium, the energies of the Me–Me interactions increase substantially on going to bis(η^6-mesitylene)chromium (see Figure 3).[62]

The 'pure' influence of the six methyl substituents estimated from the MATI data for (η^6-C_6H_6)$_2$Cr and (η^6-MeC_6H_5)(η^6-C_6H_6)Cr (see Table 1) would result in the (η^6-1,3,5-$Me_3C_6H_3$)$_2$Cr I_{ad} of 39920 cm^{-1}. The experimental ZEKE ionization energies are 40357 and 40559 cm^{-1} for the staggered (60°) and eclipsed (0°) rotamers, respectively. The Type-1 and Type-2 Me–Me influence corresponds to the I_{ad} shift of 437 cm^{-1} (5.2 kJ mol^{-1}) and 202 cm^{-1} (2.4 kJ mol^{-1}), respectively. Note that, in contrast to (η^6-toluene)chromium, for bis(η^6-mesitylene)chromium, the Type-1 influence is stronger than the Type-2 effect (see Figure 3). This is explained by the different nature of the Type-1 and Type-2 Me–Me interactions.[62]

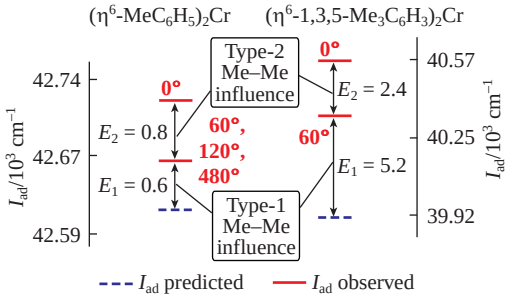

Figure 3 Predicted and observed I_{ad} values for (η^6-MeC_6H_5)$_2$Cr (left) and (η^6-1,3,5-$Me_3C_6H_3$)$_2$Cr (right). Energies E_1 and E_2 (kJ mol^{-1}) corresponding to the I_{ad} shifts caused by the Type-1 and Type-2 Me–Me mutual influence, respectively, are given. Notice the different energy scales for the two complexes. Reproduced from ref. 62 with permission from the Royal Society of Chemistry.

The influence of Me and Ph substituents on the ionization energy of (η^6-C_6H_6)$_2$Cr was compared using MATI spectroscopy.[54] The decrease in I_{ad} on going to (η^6-MeC_6H_5)(η^6-C_6H_6)Cr and (η^6-Ph_2)(η^6-C_6H_6)Cr (see Table 1) appears to be very close (695 and 713 cm^{-1}, respectively). This similarity contradicts conclusions based on the redox potentials in solution (the electrochemical studies of (η^6-Arene)$_2$Cr describe the Ph group as an electron withdrawing substituent, in contrast to the Me group).[63–65] The explanation of this discrepancy is provided by DFT calculations (*vide infra*). The ZEKE data show that the Me influence on I_{ad} of (η^6-Arene)$_2$M (M = Cr, Mo, W) is weakened on descending the group (see Table 1). On replacing two benzene ligands in (η^6-C_6H_6)$_2$M with toluene with the formation of eclipsed isomers, the ionization energy decreases by 2.90, 2.38 and 2.24% for M = Cr, Mo and W, respectively. The influence of the nature of the metal atom on the substituent effect in a sandwich molecule (see Table 1) leads to the reversed order of the (η^6-1,3,5-$Me_3C_6H_3$)$_2$Cr and (η^6-1,3,5-$Me_3C_6H_3$)$_2$W ionization energies [I_{ad} (Cr) < I_{ad} (W)] compared to those in the bisbenzene and bistoluene systems [I_{ad} (Cr) > I_{ad} (W)].[62]

The effect of the Me substituent on I_{ad} becomes stronger on going from (η^6-C_6H_6)$_2$Cr to (η^5-C_5H_5)$_2$Co. On going from unsubstituted cobaltocene[58] to methylcobaltocene,[59] I_{ad} decreases by 950 cm^{-1} (0.1178 eV), which is 36% larger than the 698 cm^{-1} (0.0865 eV) shift on monomethylation of bis(η^6-benzene)chromium.[51] Note that these fine effects become observable only with the high-resolution MATI and ZEKE techniques. There were no chances to analyze such small changes in the electronic parameters using 'classical' photoelectron spectroscopy.

Besides accurate data on the ionization energy of sandwich molecules, ZEKE/MATI experiments give unique information concerning vibrational frequencies of free sandwich ions. Vibronic structures of sandwich ZEKE/MATI spectra usually show a progression on the symmetric metal–ligand stretching mode ν_{M-L} as ionization affects the M–L distance. The corresponding wavenumbers are collected in Table 1. In the unsubstituted 3d metal complexes, they lie in the range of 228–309 cm^{-1} (see Table 1). The ν_{M-L} frequencies correlate with the nature of the ionized MO (Table 2, Figures 4, 5). The lower values correspond to the titanium and vanadium bisbenzene complexes where an electron is ionized from the bonding e_2 MO, contributed by the metal d_{xy,x^2-y^2} wavefunctions and the ligand π-orbitals (in this work, irreducible representations of the D_5 and D_6 point groups are used to denote MOs, electronic states and

Table 2 Electronic configurations and state symmetries (the D_5 or D_6 point group) of neutral and cationic sandwich complexes. The ionized orbitals are indicated.

Compound	Neutral	Cation	Ionized MO
(η^6-C_6H_6)$_2$Ti	$(e_2)^4(a_1)^0$ ($^1A_1$)	$(e_2)^3(a_1)^0$ ($^2E_2$)	e_2
(η^6-C_6H_6)$_2$V	$(e_2)^4(a_1)^1$ ($^2A_1$)	$(e_2)^3(a_1)^1$ ($^3E_2$)	e_2
(η^6-Arene)$_2$Cr	$(e_2)^4(a_1)^2$ ($^1A_1$)	$(e_2)^4(a_1)^1$ ($^2A_1$)	a_1
(η^6-Arene)$_2$Mo	$(e_2)^4(a_1)^2$ ($^1A_1$)	$(e_2)^4(a_1)^1$ ($^2A_1$)	a_1
(η^6-Arene)$_2$W	$(e_2)^4(a_1)^2$ ($^1A_1$)	$(e_2)^4(a_1)^1$ ($^2A_1$)	a_1
(η^5-C_5H_5)$_2$Fe	$(e_2)^4(a_1)^2$ ($^1A_1$)	$(e_2)^3(a_1)^2$ ($^2E_2$)	e_2
(η^5-C_5Me_5)$_2$Mn	$(e_2)^3(a_1)^2$ ($^2E_2$)	$(e_2)^3(a_1)^1$ ($^3E_2$)	a_1
(η^5-C_5H_5)$_2$Co	$(e_2)^4(a_1)^2(e_1)^1$ ($^2E_1$)	$(e_2)^4(a_1)^2$ ($^1A_1$)	e_1
(η^5-MeC_5H_4)(η^5-C_5H_5)Co	$(e_2)^4(a_1)^2(e_1)^1$ ($^2E_1$)	$(e_2)^4(a_1)^2$ ($^1A_1$)	e_1
(η^8-C_8H_8)(η^5-C_5H_5)Ti	$(e_2)^4(a_1)^1$ ($^2A_1$)	$(e_2)^4(a_1)^0$ ($^1A_1$)	a_1
(η^7-C_7H_7)(η^5-C_5H_5)Cr	$(e_2)^4(a_1)^2$ ($^1A_1$)	$(e_2)^3(a_1)^1$ ($^2A_1$)	a_1

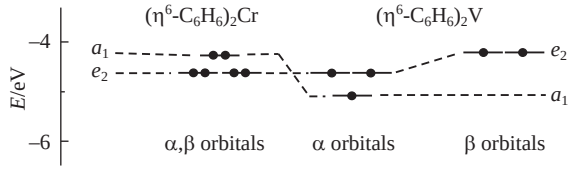

Figure 4 Calculated[66] [B3LYP/6-31++G(d,p)] energies of higher occupied MOs of $(\eta^6\text{-}C_6H_6)_2Cr$ and $(\eta^6\text{-}C_6H_6)_2V$ (the D_6 point group).

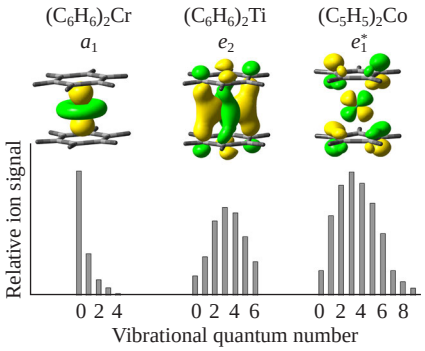

Figure 5 Isosurfaces of ionized MOs and the intensity distribution in the progression on the ν_{M-L} mode observed in the experimental MATI and ZEKE spectra of various sandwich complexes (the D_5 or D_6 point group). Reproduced from ref. 60 with permission from the Royal Society of Chemistry.

vibrational modes of sandwich molecules unless otherwise specified). The highest metal–ligand stretch frequency is associated with cobaltocene where an electron is detached from the antibonding e_1 MO, formed by the cobalt $d_{xz,yz}$ and ligand π-orbitals, and the closed-shell ion is produced. The ν_{M-L} frequencies of $(\eta^6\text{-}C_6H_6)_2Cr$ and $(\eta^7\text{-}C_7H_7)(\eta^5\text{-}C_5H_5)Cr$ with ionized non-bonding MO d_{z^2} lie in the middle of the range. A surprisingly low ν_{M-L} ion frequency is revealed by the MATI spectrum of $(\eta^8\text{-}C_8H_8)(\eta^5\text{-}C_5H_5)Ti$ where an electron is removed also from the metal d_{z^2} orbital (see Table 1). This anomaly is explained by specific metal–ligand bonding in this complex as shown by DFT calculations (*vide infra*). A replacement of Cr or Mo with W in bisarene complexes leads to a substantial increase in the ν_{M-L} ion frequency by 34–58% (see Table 1) due to a stronger relativistic effect of W that strengthens the metal–ligand bonding.

In addition to the ν_{M-L} stretching mode, the MATI and ZEKE spectra of unsubstituted sandwiches reveal weaker vibronic components. The MATI spectrum of $(\eta^6\text{-}C_6H_6)_2Cr$[48] shows many CH and ring deformation modes. The MATI signal corresponding to the ion metal–ligand unsymmetrical stretch (473 cm^{-1}) was revealed in experiments with the mixed $(\eta^7\text{-}C_7H_7)(\eta^5\text{-}C_5H_5)Cr$ sandwich.[60] The MATI spectrum of cobaltocene[58] is especially interesting due to the Jahn–Teller (JT) effect in the neutral molecule with a degenerate ground electronic state. The peaks corresponding to the JT-active out-of-plane ring distortion e_2 mode (589 cm^{-1}) were observed. The MATI spectrum of $(\eta^5\text{-}C_5H_5)_2Co$ also shows a skeletal e_1 mode (158 cm^{-1}) which testifies for the pseudo JT effect in the neutral molecule.[58]

Methylation of the rings in sandwich molecules leads to the appearance of new vibronic signals in the MATI and ZEKE spectra. In particular, the peaks arising from the Me out-of-plane bending mode were observed in the spectra of $(\eta^6\text{-}MeC_6H_5)(\eta^6\text{-}C_6H_6)Cr$ (198 cm^{-1}),[51] $(\eta^6\text{-}MeC_6H_5)_2Cr$ (166, 176, 192 and 223 cm^{-1} for the 180, 120, 60 and 0° rotamers, respectively),[52,53] $(\eta^6\text{-}1,3,5\text{-}Me_3C_6H_3)_2Cr$ (142 and 186 cm^{-1} for the 60 and 0° rotamers, respectively)[56] and $(\eta^5\text{-}C_5H_4Me)(\eta^5\text{-}C_5H_5)Co$ (219 cm^{-1}).[59] Note that there are no other methods that provide direct experimental information on the vibrational frequencies of free sandwich ions.

The ZEKE and MATI vibronic structures reflect the transformations of sandwich molecular geometry on ionization. The intensity distribution in the ν_{M-L} progression depends on the change in the metal–ligand distance. This change is small in bisarene complexes of the Group 6 metals where the non-bonding d_{z^2} orbital is ionized. Accordingly, the strongest peak in the MATI and ZEKE spectra of these compounds corresponds to the origin (the 0–0 transition) so the vertical and adiabatic ionization energies coincide (see Figure 5). The detachment of an electron from bonding MO e_2 or antibonding MO e_1 results in stronger variations of the metal–ligand distance and different intensity distributions (see Figure 5). Therefore, the vertical ionization energies of $(\eta^6\text{-}C_6H_6)_2Ti$ and $(\eta^5\text{-}C_5H_5)_2Co$ are higher than the I_{ad} values. This regularity is contradicted by the behavior of $(\eta^8\text{-}C_8H_8Me)(\eta^5\text{-}C_5H_5)Ti$,[60] where the non-bonding $3d_{z^2}$ electron is ionized but the MATI intensity distribution resembles that in $(\eta^5\text{-}C_5H_5)_2Co$. The explanation can be obtained on the basis of DFT.

Thus, it becomes clear that DFT calculations represent a necessary complement to the MATI and ZEKE studies of sandwich complexes. Computational data help to interpret the structures of the spectra and identify structure–property relationships responsible for trends in ionization energies and structural changes in sandwich molecules during ionization. On the other hand, the accurate experimental ionization energies, ion vibrational frequencies and relative vibronic intensities provided by the MATI and ZEKE spectra form a unique reference basis for validating quantum chemical calculations of sandwich complexes.

DFT simulation of ZEKE/MATI spectra of sandwich complexes

Calculated energies of optimized neutral and ion sandwich structures give the I_{ad} values which depend on the functional and basis set used. Various DFT levels were tested using high-resolution ionization energy of bis(η^6-benzene)chromium.[67] The smallest difference between the DFT and MATI I_{ad} was obtained with the 'old' non-hybrid BPW91 functional and triple-ζ TZVP basis set (Table 3). The use of the double-ζ basis set 6-31g(d) in combination with both hybrid and 'pure' functionals leads to a large underestimation of ionization energy of $(\eta^6\text{-}C_6H_6)_2Cr$.

Good agreement between the theoretical and experimental I_{ad} values was achieved at the BPW91/TZVP level of DFT for cobaltocene and methylcobaltocene.[58,59] A small deviation of the calculated parameter was also obtained with the meta-hybrid TPSSh functional (Table 4). In contrast to $(\eta^6\text{-}C_6H_6)_2Cr$, for $(\eta^5\text{-}C_5H_5)_2Co$, the B3PW91 and B3LYP hybrid functionals overestimate I_{ad} by 1500–2600 cm^{-1}. DFT calculations at the

Table 3 I_{ad} values (cm^{-1}) of $(\eta^6\text{-}C_6H_6)_2Cr$ calculated[67] with various combinations of functionals and basis sets. The differences between the calculated and experimental values are given in parentheses.

Basis set	B3LYP[a]	MPW1PW91[a]	B3PW91[a]	BPW91[b]
6-31G(d)[c]	41860	–	41699	41860
	(–2227)		(–2388)	(–2227)
6-311+G(d,p)[d]	43715	43312	43715	43715
	(–372)	(–775)	(–372)	(–372)
DGDZVP[c]	43876	43634	43957	43876
	(–211)	(–453)	(–130)	(–211)
TZVP[d]	43715	43312	43715	44118
	(–372)	(–775)	(372)	(31)

[a] A hybrid functional. [b] A 'pure' functional. [c] A double-ζ basis set. [d] A triple-ζ basis set.

Table 4 Adiabatic ionization energy values (cm^{-1}) of $(\eta^5\text{-}C_5H_4Me)(\eta^5\text{-}C_5H_5)_2Co$/$(\eta^5\text{-}C_5H_5)_2Co$ (I_{ad}^{calc}) calculated at various levels of theory,[59] their deviations from the experimental MATI data ($\Delta I^{calc-exp}$) and the change of the cobaltocene ionization energy upon methylation (ΔI_{Me}).

Level of theory	I_{ad}^{calc}	$\Delta I^{calc-exp}$	ΔI_{Me}
BPW91/TZVP	42392/41295	–573/–726	–1097
B3PW91/6-311+G(d,p)	44820/43755	1855/1734	–1065
B3PW91/6-311++G(d,p)	44812/43763	1847/1742	–1049
B3LYP/6-311++G(d,p)	45546/44497	2581/2476	–1049
TPSSh/6-311+G(d,p)	42562/41521	–411/–500	–1040
CCSD(T)/cc-pVDZ	41723/40747	–1250/–1274	–976
CCSD(T)/cc-pVTZ	43086/42110	121/89	–976

BPW91/TZVP and TPSSh/6-311+G(d,p) levels of theory appear to give even better results than coupled cluster CCSD(T)/cc-pVDZ computations though the CCSD(T)/cc-pVTZ level of theory is superior to DFT (Table 4).

The experimental 952 cm^{-1} red shift of I_{ad} on methylation of cobaltocene, ΔI_{Me}, is *ca.* 10% lower than that estimated by DFT (1040–1097 cm^{-1}) while the coupled cluster method gives a very close shift of 976 cm^{-1} (see Table 4). A similar slight overestimation of ΔI_{Me} by DFT (85 cm^{-1}) was obtained with $(\eta^6\text{-}MeC_6H_5)(\eta^6\text{-}C_6H_6)Cr$.[51] DFT calculations were successfully used to analyze the substituent effects in chromium bisarene complexes. These computations made it possible to explain why the influence of the Ph and Me groups on the oxidation of free sandwich molecules is the same, and the influence of the Me and Ph fragments on the redox potential of the $(\eta^6\text{-Arene})_2Cr^{+/0}$ couple in solution is opposite (the latter arises from solvation effects but not intramolecular interactions).[54] Therefore, despite the fact that good performance of DFT is often considered as a result of error cancellation,[68] this approach provides a fast and fairly accurate estimate of sandwich adiabatic ionization energies.

DFT calculations also provide reliable vibrational frequencies of sandwich cations, which form the basis for interpreting the vibronic structures of MATI and ZEKE spectra. Similar to ionization energies, the 'pure' BPW91 functional demonstrates good performance when calculating frequencies of the $(\eta^6\text{-}C_6H_6)_2Cr^+$ vibrations.[67] There is an excellent linear correlation between the BPW91/TZVP[67] and MATI[48] vibrational frequencies of the $(\eta^6\text{-}C_6H_6)_2Cr^+$ ion (Figure 6). This level of calculations can be used without frequency scaling. Not-scaled DFT (BPW91, B3LYP and B3PW91) frequencies of normal vibrations were also used to model the ZEKE or MATI spectra of $(\eta^6\text{-}C_6H_6)_2M$ (M = Ti, V)[45] substituted derivatives of $(\eta^6\text{-}C_6H_6)_2M$ (M = Cr, Mo, W),[51,53,54,56] metallocenes,[57–59] and mixed sandwich complexes.[60]

Not only vibrational frequencies of sandwich molecules but also the intensity distribution in the ZEKE and MATI vibronic structures can be reproduced by DFT calculations. The

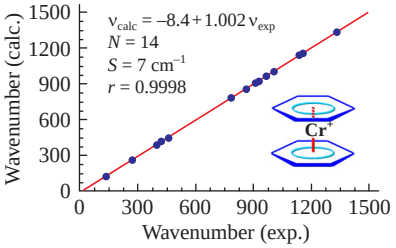

Figure 6 Linear correlation between calculated (BPW91/TZVP)[67] and experimental (MATI)[48] vibrational frequencies. The correlation parameters are given (N is the number of points, S standard error and r correlation coefficient).

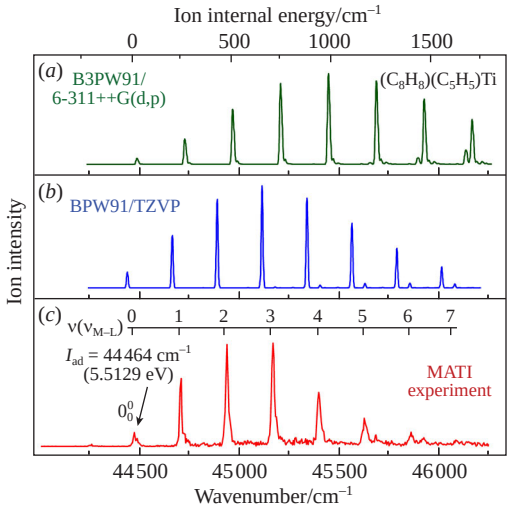

Figure 7 (*a*), (*b*) Simulated and (*c*) experimental MATI spectra of $(\eta^8\text{-}C_8H_8)(\eta^5\text{-}C_5H_5)Ti$. Vibrational quantum numbers corresponding to the excitation of the metal–ligand symmetric stretch ν_{M-L} in the cation are given. Reproduced from ref. 60 with permission from the Royal Society of Chemistry.

simulations of MATI and ZEKE spectra are based on the computations of Franck–Condon factors following the optimization and vibrational analysis of neutrals and ions. The theoretical spectra agree well with the experiments for all sandwich systems studied. In particular, DFT calculations reproduce the anomalous MATI vibronic structure of $(\eta^8\text{-}C_8H_8)(\eta^5\text{-}C_5H_5)Ti$[60] with a long progression on the metal–ligand stretching mode, the 'pure' BPW91 functional producing a better intensity distribution than the B3PW91 hybrid (Figure 7). The BPW91 calculations are also superior to B3PW91 when describing the ν_{M-L} progression in the MATI spectra of cobaltocene[58,69] and methylcobaltocene.[59] The popular B3LYP functional predicts a too long progression in the MATI spectrum of $(\eta^5\text{-}C_5H_4Me)(\eta^5\text{-}C_5H_5)Co$ (Figure 8). On the other hand, the B3PW91 hybrid functional describes relative intensities of some weaker vibronic components in the MATI spectrum of cobaltocene[69] and methylcobaltocene[59] better than BPW91 (see Figure 8). Interestingly, DFT well reproduces the $(\eta^5\text{-}C_5H_5)_2Co$

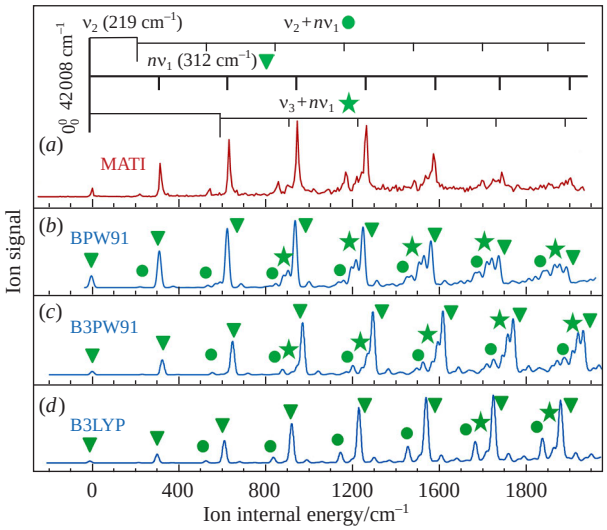

Figure 8 (*a*) Experimental MATI spectrum of $(\eta^5\text{-}C_5H_4Me)(\eta^5\text{-}C_5H_5)Co$ and its simulation at the (*b*) BPW91/TZVP, (*c*) B3PW91/6-311++G(d,p) and (*d*) B3LYP/6-311++G(d,p) levels of DFT. The zero wavenumber corresponds to the position of the origin. The vibronic components arising from the excitation of the metal–ligand stretch (ν_1), Me bend (ν_2) and out-of-plane ring deformation (ν_3) in the ion are indicated. Reproduced from ref. 59 with permission from the PCCP Owner Societies.

MATI peaks corresponding to the excitation of the JT active out-of-plane ring distortion e_2 mode but not pseudo JT skeletal e_1 mode.[69] The vibronic intensities in the MATI and ZEKE spectra of sandwich molecules can be correlated with the structural transformations accompanying ionization. The good quality of modeling spectra with DFT indicates a reliable description of these transformations by calculations.

Changes in the molecular and electronic structures of sandwich molecules on ionization

The vibrational progression on the symmetric $\nu_{M–L}$ mode in the MATI and ZEKE spectra of sandwich complexes is indicative of variations in the metal–ligand distances on ionization. Calculated metal–ring and ring–ring distances in the neutral and ion species are given in Table 5. Upon ionization, the distances increase in ferrocene where the bonding e_2 electron is detached and decrease in cobaltocene or methylcobaltocene where the antibonding e_1 orbital is ionized. An elongation of some M–C distances by *ca.* 0.1 Å on going from neutrals to ground-state ions was predicted by DFT calculations of $(\eta^6\text{-}C_6H_6)_2M$ (M = Ti, V; ionized orbital e_2) which agrees with the intensity distribution in the ZEKE $\nu_{M–L}$ progression.[45]

On the other hand, the a_1 (d_{z^2}) ionization can lead to various changes in the interligand distances. The ligand separation remains unchanged in $(\eta^7\text{-}C_7H_7)(\eta^5\text{-}C_5H_5)Cr$, increases by 0.03–0.05 Å in $(\eta^6\text{-}C_6H_6)_2Cr$ and $(\eta^5\text{-}C_5Me_5)_2Mn$, and decreases by 0.16–0.18 Å in $(\eta^8\text{-}C_8H_8)(\eta^5\text{-}C_5H_5)Ti$ (see Table 5). Surprisingly, in the latter case, the decrease in the metal–ring and ring–ring distances is close to that in cobaltocene where the antibonding e_1 electron is ionized. However, this structural variation correlates well with the long $\nu_{M–L}$ progression in the MATI spectrum of $(\eta^8\text{-}C_8H_8)(\eta^5\text{-}C_5H_5)Ti$ reproduced by DFT calculations (see Figure 7). The calculated shortening of the ring–ring separation in $(\eta^8\text{-}C_8H_8)(\eta^5\text{-}C_5H_5)Ti$ agrees also with that observed in the single crystals of the titanium *ansa*-derivative bearing bridged cyclooctateraene and cyclopentadienyl ligands (*ca.* 0.20 Å).[70] Various structural changes caused by the removal of a nonbonding a_1 electron show that the orbital nature cannot serve as the only criterion in predicting geometric transformations of sandwich molecules on ionization.

The electron detachment from methylated neutral sandwich complexes leads to excitation of the Me bending mode. The corresponding components appear in the vibronic structures of MATI and ZEKE spectra. However, the Me bending angle difference between the neutral and the ion is usually negligible. For instance, in $(\eta^5\text{-}C_5Me_5)_2Mn$, the B3PW91/6-311++G(d,p) ring centroid–C_{ring}–C_{Me} angles change by only 0.1–0.6° on ionization.[57] Therefore, the excitation of the Me bending vibration on ionization of methylated sandwiches is associated with the change in the metal–ring distances and, therefore, the metal–Me distances, rather than with the variation of the equilibrium Me bending angle itself.

In cobaltocene, the geometry transformations on ionization involve distortions of the C_5 rings. This is caused by the JT effect in the neutral molecule with the singly occupied component of the $3d_{xz,yz}/\pi$ orbital which is degenerate (e_1'') in the D_{5h} point group. Vibronic interactions reduce the molecular symmetry to C_{2v}. As a result, the $^2E_1''$ (D_{5h}) degenerate ground electronic state splits into the $^2A_2$ and $^2B_1$ components (C_{2v}) and the potential energy surface takes on the well-known 'Mexican hat' shape. The JT energy parameters are shown in Figure 9. According to DFT calculations,[71] the largest contribution to the JT stabilization energy E_{JT} is provided by the ring out-of-plane deformation mode (587 cm^{-1}) belonging to the e_2' type in the D_{5h} point group. On going to the C_{2v} group, this vibration splits into the a_1 and b_2 components, the former corresponding to normal coordinate Q_a (see Figure 9). Component b_2 is responsible for the pseudorotation of the system along the 'Mexican hat' moat. The Δ energy difference (see Figure 9) between the two minima on the cross-section of the $(\eta^5\text{-}C_5H_5)_2Co^0$ potential energy surface (PES) is negligible (<1 cm^{-1}) [59,71] so the pseudorotation is barrierless and the effective symmetry of the molecule remains D_{5h}. Despite this, the MATI spectrum of cobaltocene[58] 'feels' the JT distortion

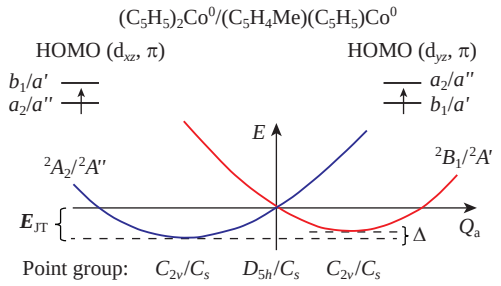

Figure 9 Cross-section of the $(\eta^5\text{-}C_5H_5)_2Co^0/(\eta^5\text{-}C_5H_4Me)(\eta^5\text{-}C_5H_5)Co^0$ PES along coordinate Q_a of the totally symmetric component of the JT-active vibration. The corresponding point groups, frontier α-MOs and JT energy parameters are given. Reproduced from ref. 59 with permission from the PCCP Owner Societies.

Table 5 Calculated BPW91/B3PW91 metal–ring centroid and ring centroid–ring centroid distances (Å) in sandwich neutrals and cations and differences between them Δ*r*. The ionized MO (the D_5 or D_6 point group) is indicated for each complex in parentheses.

Compound (ionized MO)	Distance	$r_{neutral}$	r_{cation}	Δ*r*
$(\eta^5\text{-}C_5H_5)_2Co^a$ (e_1)	Co–C_5	1.735/1.737	1.659/1.644	–0.076/–0.093
	C_5–C_5	3.470/3.474	3.318/3.288	–0.152/–0.186
$(\eta^5\text{-}C_5H_4Me)(\eta^5\text{-}C_5H_5)Co^a$ (e_1)	C_5–C_5	3.437/–	3.321/–	–0.116/–
$(\eta^5\text{-}C_5H_5)_2Fe^b$ (e_2)	Fe–C_5	1.654/1.651	1.730/1.716	0.076/0.065
	C_5–C_5	3.308/3.302	3.460/3.432	0.152/0.130
$(\eta^5\text{-}C_5Me_5)_2Mn^c$ (a_1)	Mn–C_5	–/1.747	–/1.771	–/0.024
	C_5–C_5	–/3.494	–/3.542	–/0.048
$(\eta^6\text{-}C_6H_6)_2Cr^d$ (a_1)	Cr–C_6	1.621/1.609	1.640/1.626	0.019/0.017
	C_6–C_6	3.242/3.218	3.280/3.252	0.038/0.034
$(\eta^7\text{-}C_7H_7)(\eta^5\text{-}C_5H_5)Cr^d$ (a_1)	Cr–C_7	1.443/1.414	1.441/1.419	–0.002/0.005
	Cr–C_5	1.830/1.827	1.826/1.810	–0.004/–0.017
	C_7–C_5	3.273/3.241	3.267/3.229	–0.006/–0.012
$(\eta^8\text{-}C_8H_8)(\eta^5\text{-}C_5H_5)Ti^d$ (a_1)	Ti–C_8	1.476/1.448	1.373/1.340	–0.103/–0.108
	Ti–C_5	2.045/2.033	1.991/1.966	–0.054/–0.067
	C_8–C_5	3.521/3.481	3.364/3.306	–0.157/–0.175

[a] Ref. 59. [b] Ref. 69. [c] Ref. 57. [d] Ref. 60.

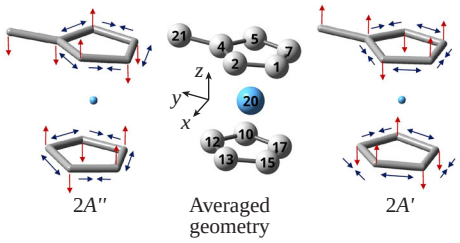

Figure 10 Shifts of the carbon atoms and variations of the C–C bond lengths accompanying the vibronic structural distortions of neutral methylcobaltocene (the C_s point group). The red and blue arrows denote the out-of-plane atomic shifts and the changes of the C–C bond lengths, respectively. Reproduced from ref. 59 with permission from the PCCP Owner Societies.

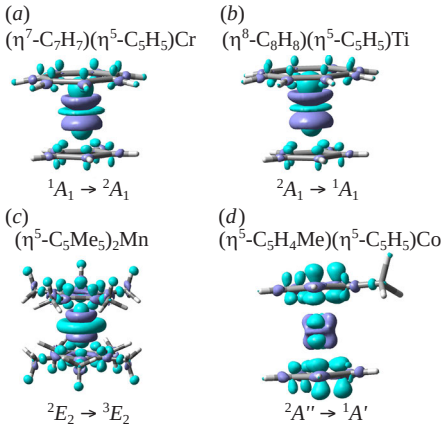

Figure 11 Calculated EDD isosurfaces (isovalue 0.003 a.u.) corresponding to ionization of (*a*) $(\eta^7\text{-}C_7H_7)(\eta^5\text{-}C_5H_5)Cr$, (*b*) $(\eta^8\text{-}C_8H_8)(\eta^5\text{-}C_5H_5)Ti$, (*c*) $(\eta^5\text{-}C_5Me_5)_2Mn$ and (*d*) $(\eta^5\text{-}C_5H_4Me)(\eta^5\text{-}C_5H_5)Co$. The violet and blue colors indicate the positive and negative EDD values, respectively. Electronic transitions are denoted using irreducible representations of the D_5 (*a*)–(*c*) and C_s (*d*) point groups.

and shows clearly defined vibronic peaks corresponding to the out-of-plane ring deformation mode. This demonstrates the extremely high sensitivity of the laser threshold ionization spectra to the structural changes in sandwich molecules.

Methylation of the cobaltocene C_5H_5 ring leads to nonequivalence of the $3d_{xz}/\pi$ and $3d_{yz}/\pi$ orbital energies. The $(\eta^5\text{-}C_5H_4Me)(\eta^5\text{-}C_5H_5)Co^0$ molecule belongs to the C_s point group so its ground electronic state is formally nondegenerate. Nevertheless, the $^2A''$ and $^2A'$ potential energy curves intersect and the PES cross-section qualitative diagram (see Figure 9) remains unchanged. However, the calculated Δ parameter increases by *ca*. 180 cm^{-1} upon methylation so the pseudorotation becomes hindered in methylcobaltocene.[59] The $^2A''$ minimum (see Figure 9) is a true minimum, while the $^2A'$ extreme corresponds to a saddle point on the 3-D PES. The computed[59] atomic shifts during the transition from the averaged structure near the $^2A''/^2A'$ conical intersection to the PES extrema are shown in Figure 10. It is seen that not only out-of-plane ring distortions but also in-plane ring deformations are caused by vibronic interactions. The latter are similar to those in the $C_5H_5^{\bullet}$ radical which can adopt an allylic or diene structure.[72–75]

On going from the neutral to the ion, the rings of methylcobaltocene become planar and the C_{ring}–C_{ring} bond lengths – nearly equal.[59] As a consequence, the MATI spectrum reveals the out-of-plane deformation mode. The vibronic components corresponding to the in-plane ring distortion are not observed due to low intensities and overlapping with the stronger combination bands arising from excitations of other modes.[59]

The in-plane ring deformations were found also in neutral decamethylmanganocene which would have a $^2E_2$ degenerate ground electronic state under the D_5 symmetry.[57] However, the electronic symmetry of $(\eta^5\text{-}C_5Me_5)_2Mn$ does not change on ionization (the d_{z^2} electron is ionized) so only totally symmetric vibrations were revealed in the experimental and simulated MATI spectrum.[57] The JT distortion of decamethylmanganocene differs from that of cobaltocene due to the different nature of the singly-occupied MO. In $(\eta^5\text{-}C_5Me_5)_2Mn^0$, the unpaired electron occupies MO d_{xy} or $d_{x^2-y^2}$ belonging to the e_2 set in a non-distorted molecule. In $(\eta^5\text{-}C_5H_5)_2Co^0$, the single-occupied MO is derived from the Co d_{xz} or d_{yz} and ligand $\pi(e_1)$ wavefunctions (see Table 2). Structural changes accompanying the detachment of an electron from sandwich molecules are associated with a redistribution of the charge density upon ionization.

The deformations of electron density (ED) on going from neutral sandwiches to ions are well visualized by the ED difference (EDD) isosurfaces shown in Figure 11 for selected metallocenes and heteroligand complexes. They were built at the B3PW91/6-311++G(d,p) level of theory on the basis of the optimized molecular geometries published elsewhere.[57,59,60] These isosurfaces reveal inhomogeneous ED variations during ionization. There are areas of both negative and positive EDD in the vicinity of the metal atom. The shapes of the negative EDD isosurfaces correspond to the ionized MOs. The difference between methylcobaltocene (MO d_{xz}/π) and other complexes (MO d_{z^2}) is clearly seen. The local increase in ED upon ionization of sandwich molecules is counterintuitive but its nature can be understood on the basis of the charge distribution analysis.

The atomic charges in selected neutral and ionic sandwich systems calculated[57,59,60] within the frames of Bader's quantum theory of atoms in molecules (QTAIM)[76,77] are given in Table 5. It is seen that ionization is accompanied by a substantial ED transfer from the ligands to the metal. As a result, the d_{z^2} ionization causes an increase in the metal atomic charges by only 0.15–0.20 a.u. despite the metal-localized nature of the ionized orbital. A similar conclusion was made earlier on the basis of semiempirical[78,79] and multiple scattering Xα[80] calculations of bis(η^6-benzene)chromium. A negligible change in the metal charge (0.01–0.02 a.u.) corresponds to the d_{xz}/π ionization of cobaltocene and methylcobaltocene (see Table 5). Therefore, the ED relaxation after the electron detachment is responsible for the positive EDD areas around the nodal surfaces of the ionized MO (see Figure 11).

Some ED increase during ionization is found also in the vicinity of the C–C and C–H σ-bonds (see Figure 11). This

Table 6 Calculated[a] QTAIM charges *q* (a.u.) on the fragments of neutral and ionic sandwich complexes at their equilibrium geometries. Charge variations on ionization Δ*q* are also presented.

Compound	Fragment	$q_{neutral}$	q_{cation}	Δ*q*
$(\eta^5\text{-}C_5H_5)_2Co$[b]	Co	0.74	0.75	0.01
	C_5H_5	–0.37	0.12	0.49
$(\eta^5\text{-}C_5H_4Me)(\eta^5\text{-}C_5H_5)Co$[b]	Co	0.73	0.75	0.02
	C_5H_5	–0.38	0.10	0.48
	C_5H_4Me	–0.35	0.15	0.50
$(\eta^5\text{-}C_5Me_5)_2Mn$[c]	Mn	0.87	1.07	0.20
	C_5Me_5	–0.44	–0.04	0.40
$(\eta^6\text{-}C_6H_6)_2Cr$[d]	Cr	0.95	1.14	0.19
	C_6H_6	–0.48	–0.07	0.41
$(\eta^7\text{-}C_7H_7)(\eta^5\text{-}C_5H_5)Cr$[d]	Cr	1.06	1.22	0.16
	C_7H_7	–0.61	–0.10	0.51
	C_5H_5	–0.46	–0.12	0.34
$(\eta^8\text{-}C_8H_8)(\eta^5\text{-}C_5H_5)Ti$[d]	Ti	1.46	1.64	0.18
	C_8H_8	–0.91	–0.40	0.51
	C_5H_5	–0.55	–0.24	0.31

[a] The B3PW91/6-311++G(d,p) level of DFT. [b] Ref. 59. [c] Ref. 57. [d] Ref. 60.

effect partially compensates for the loss of negative charge on the carbon atoms. As a result, the main total contribution to the ED loss upon ionization is provided by the hydrogen atoms of the ligands, which is also confirmed by the more accurate coupled cluster calculations of methylcobaltocene.[59]

Comparison of metal QTAIM charges in sandwich (see Table 5) shows that titanium in neutral $(\eta^8\text{-}C_8H_8)(\eta^5\text{-}C_5H_5)Ti$ bears a substantially larger positive charge (1.46 a.u.) than the metals in other compounds (0.73–1.06 a.u.). This testifies for more ionic metal–ligand interactions in $(\eta^8\text{-}C_8H_8)(\eta^5\text{-}C_5H_5)Ti$. The higher ionic contribution to the metal–ligand bonds is responsible for the anomalous structural behavior of the mixed titanium complex on ionization[60] and the extremely long MATI vibrational progression described above (see Figure 7). Thus, the results of DFT calculations explain very well the specific effects observed in the experimental threshold ionization spectra of sandwich molecules.

Conclusions and outlook

The laser threshold ionization techniques using jet-cooled molecular beams provide much more accurate data on ionization energies of sandwich complexes as compared to 'classical' photoelectron spectroscopy. In addition, unique information about the vibrational frequencies of sandwich cations as well as structural changes in sandwich molecules during ionization can be obtained from the MATI and ZEKE spectra. Fine substituent effects were discovered, including the energy non-equivalence of sandwich rotational conformers and mutual influence of the introduced groups. These experimental data form a reliable basis for validation of the results of quantum chemical calculations. The performance of various DFT levels can be efficiently tested. On the other hand, DFT calculations make it possible to interpret the MATI and ZEKE vibronic structures, describe structural changes in sandwich molecules during ionization and unveil mechanisms of intramolecular interactions. Therefore, MATI and ZEKE spectroscopies supported by DFT calculations provide extremely powerful tools for studying new aspects of the electronic structure of sandwich complexes. Further MATI/ZEKE investigations of transition-metal sandwich systems can deal with the compounds bearing functional organic groups or heavier congeners of 3d metals. For metallocenes with relatively high ionization energies, such as manganocene, ferrocene and nickelocene, threshold ionization techniques using vacuum UV irradiation sources[81–83] can be employed. High-resolution experimental data will be useful for testing not only fast DFT calculations of sandwich molecules but also more accurate multi-configurational and multi-reference computational methods.[84–90]

This work was supported by the Russian Science Foundation (project no. 23-13-00139, https://rscf.ru/project/23-13-00139/).

References

1 G. Wilkinson, M. Rosenblum, M. C. Whiting and R. B. Woodward, *J. Am. Chem. Soc.*, 1952, **74**, 2125.
2 E. O. Fischer and W. Pfab, *Z. Naturforsch.*, 1952, **7**, 377.
3 E. O. Fischer and W. Hafner, *Z. Naturforsch.*, 1955, **10**, 665.
4 *The Nobel Prize in Chemistry 1973*, https://www.nobelprize.org/prizes/chemistry/1973/summary/.
5 D. Seyferth, *Organometallics*, 2002, **21**, 2800.
6 C. Elschenbroich, in *Organometallics*, 3rd edn., Wiley-VCH, Weinheim, 2006, ch. 15, pp. 528–549.
7 T. N. Gribanova, R. M. Minyaev and V. I. Minkin, *Mendeleev Commun.*, 2023, **33**, 302.
8 F. G. N. Cloke, J. C. Green, A. F. R. Kilpatrick and D. O'Hare, *Coord. Chem. Rev.*, 2017, **344**, 238.
9 H. Braunschweig, A. Damme, S. Demeshko, K. Duck, T. Kramer, I. Krummenacher, F. Meyer, K. Radacki, S. Stellwag-Konertz and G. R. Whittell, *J. Am. Chem. Soc.*, 2015, **137**, 1492.
10 R. A. Musgrave, A. D. Russell, D. W. Hayward, G. R. Whittell, P. G. Lawrence, P. J. Gates, J. C. Green and I. Manners, *Nat. Chem.*, 2017, **9**, 743.
11 D. Astruc, *Chem. Commun.*, 2023, **59**, 7321.
12 J.-C. Eloi, L. Chabanne, G. R. Whittell and I. Manners, *Mater. Today*, 2008, **11**, 28.
13 Y. Wang, D. Astruc and A. S. Abd-El-Aziz, *Chem. Soc. Rev.*, 2019, **48**, 558.
14 G. Gritzner, in *Handbook of Reference Electrodes*, eds. G. Inzelt, A. Lewenstam and F. Scholz, Springer, Berlin, 2013, ch. 2, pp. 25–31.
15 J. Jörissen and B. Speiser, in *Organic Electrochemistry: Revised and Expanded*, 5th edn., eds. O. Hammerich and B. Speiser, CRC Press, Boca Raton, 2015, ch. 7, pp. 263–330.
16 Y. Ding, C. Zhang, L. Zhang, Y. Zhou and G. Yu, *Chem. Soc. Rev.*, 2018, **47**, 69.
17 K. Liu, Y. Liu, D. Lin, A. Pei and Y. Cui, *Sci. Adv.*, 2018, **4**, 9820.
18 D. Astruc, *Organometallic Chemistry and Catalysis*, Springer, Berlin, 2007, ch. 11, pp. 251–288.
19 M. P. Boone and D. W. Stephan, *J. Am. Chem. Soc.*, 2013, **135**, 8508.
20 M. Bochmann, *Organometallics and Catalysis: An Introduction*, Oxford University Press, Oxford, 2015.
21 R. Liu, S. H. Ke, H. U. Baranger and W. Yang, *Nano Lett.*, 2005, **5**, 1959.
22 Y. Ji, H. Lv and X. Wu, *Nanoscale Adv.*, 2024, **6**, 985.
23 C. Morari, I. Rungger, A. R. Rocha, S. Sanvito, S. Melinte and G.-M. Rignanese, *ACS Nano*, 2009, **3**, 4137.
24 P. Plachida, D. R. Evans and R. Solanki, in *Nanoelectronic Device Applications Handbook*, eds. J. E. Morris and K. Iniewski, CRC Press, Boca Raton, 2013, ch. 32, pp. 409–420.
25 M. S. Inkpen, A. J. P. White, T. Albrecht and N. J. Long, *Dalton Trans.*, 2014, **43**, 15287.
26 L. E. Wilson, C. Hassenrück, R. F. Winter, A. J. P. White, T. Albrecht and N. J. Long, *Angew. Chem., Int. Ed.*, 2017, **56**, 6838.
27 A. Ghosh, S. Mishra, S. Giri, S. M. Mobin, A. Bera and S. Chatterjee, *Organometallics*, 2018, **37**, 1999.
28 D. R. van Staveren and N. Metzler-Nolte, *Chem. Rev.*, 2004, **104**, 5931.
29 T. Ihara, in *Advances in Bioorganometallic Chemistry*, 1st edn., eds. T. Hirao and T. Moriuchi, Elsevier, Amsterdam, 2019, ch. 14, pp. 277–303.
30 B. Albada and N. Metzler-Nolte, *Chem. Rev.*, 2016, **116**, 11797.
31 M. Patra and G. Gasser, *Nat. Rev. Chem.*, 2017, **1**, 0066.
32 R. Das, D. R. Chatterjee and A. Shard, *Coord. Chem. Rev.*, 2024, **504**, 215666.
33 J. C. Green, *Struct. Bonding*, 1981, **43**, 37.
34 L. P. Yur'eva, S. M. Peregudova, D. N. Kravtsov, A. Yu. Vasil'kov, L. N. Nekrasov, N. L. Asfandiarov, M. M. Timoshenko and Yu. V. Chizhov, *J. Organomet. Chem.*, 1987, **336**, 371.
35 J. C. Green, M. L. H. Green, N. Kaltsoyannis, P. Mountford, P. Scott and S. J. Simpson, *Organometallics*, 1992, **11**, 3353.
36 J. G. Brennan, G. Cooper, J. C. Green, N. Kaltsoyannis, M. A. MacDonald, M. P. Payne, C. M. Redfern and K. H. Sze, *Chem. Phys.*, 1992, **164**, 271.
37 L. Li, J. Zhang, C. Yang, L. Huang, J. Zhang, J. Bai, C. Redshaw, X. Feng, C. Cao, N. Huo, J. Li and B. Z. Tang, *Small*, 2021, **17**, 2103125.
38 S. K. Sahoo, *Dalton Trans.*, 2021, **50**, 11681.
39 A. Pal, S. R. Bhatta and A. Thakur, *Coord. Chem. Rev.*, 2021, **431**, 213685.
40 S. Giri and I. Dash, *J. Mater. Chem. A*, 2023, **11**, 16458.
41 C. Li, C. Zhang, J. Xie, K. Wang, J. Li and Q. Zhang, *Chem. Eng. J.*, 2021, **404**, 126463.
42 G. Roy, R. Gupta, S. R. Sahoo, S. Saha, D. Asthana and P. C. Mondal, *Coord. Chem. Rev.*, 2022, **473**, 214816.
43 E. W. Schlag, *ZEKE Spectroscopy*, Cambridge University Press, Cambridge, 1998.
44 D.-S. Yang, *J. Phys. Chem. Lett.*, 2011, **2**, 25.
45 B. R. Sohnlein, Y. Lei and D.-S. Yang, *J. Chem. Phys.*, 2007, **127**, 114302.
46 S. Y. Ketkov, H. L. Selzle and E. W. Schlag, *Mol. Phys.*, 2004, **102**, 1749.
47 K.-W. Choi, S. K. Kim, D.-S. Ahn and S. Lee, *J. Phys. Chem. A*, 2004, **108**, 11292.
48 K.-W. Choi, S. Choi, S. J. Baek and S. K. Kim, *J. Chem. Phys.*, 2007, **126**, 034308.
49 B. R. Sohnlein and D.-S. Yang, *J. Chem. Phys.*, 2006, **124**, 134305.
50 S. Y. Ketkov, H. L. Selzle and E. W. Schlag, *Organometallics*, 2006, **25**, 1712.

51 S. Y. Ketkov, G. V. Markin, S.-Y. Tzeng and W.-B. Tzeng, *Chem. – Eur. J.*, 2016, **22**, 4690.
52 S. Y. Ketkov, H. L. Selzle and F. G. N. Cloke, *Angew. Chem., Int. Ed.*, 2007, **46**, 7072.
53 J. S. Lee, S. Kumari and D.-S. Yang, *J. Phys. Chem. A*, 2010, **114**, 11277.
54 S. Y. Ketkov, S.-Y. Tzeng, P.-Y. Wu, G. V. Markin and W.-B. Tzeng, *Chem. – Eur. J.*, 2017, **23**, 13669.
55 S. Y. Ketkov, H. L. Selzle, F. G. N. Cloke, G. V. Markin, Y. A. Schevelev, G. A. Domrachev and E. W. Schlag, *J. Phys. Chem. A*, 2010, **114**, 11298.
56 S. Kumari and D.-S. Yang, *J. Phys. Chem. A*, 2013, **117**, 13336.
57 S. Ketkov, S.-Y. Tzeng, E. Rychagova and W.-B. Tzeng, *Molecules*, 2022, **27**, 6226.
58 S. Y. Ketkov and H. L. Selzle, *Angew. Chem., Int. Ed.*, 2012, **51**, 11527.
59 S. Y. Ketkov, S.-Y. Tzeng, E. A. Rychagova, A. Lukoyanov and W.-B. Tzeng, *Phys. Chem. Chem. Phys.*, 2024, **26**, 1046.
60 S. Y. Ketkov, S.-Y. Tzeng, E. A. Rychagova, G. V. Markin, S. G. Makarov and W.-B. Tzeng, *Dalton Trans.*, 2021, **50**, 10729.
61 S. Y. Ketkov and J. C. Green, *J. Chem. Soc., Faraday Trans.*, 1997, **93**, 2467.
62 S. Y. Ketkov, *Dalton Trans*., 2020, **49**, 569.
63 T. T.-T. Li and C. H. Brubaker, *J. Organomet. Chem.*, 1981, **216**, 223.
64 L. P. Yur'eva, S. M. Peregudova, L. N. Nekrasov, A. P. Korotkov, N. N. Zaitseva, N. V. Zakurin and A. Yu. Vasil'kov, *J. Organomet. Chem.*, 1981, **219**, 43.
65 L. P. Yur'eva, L. N. Nekrasov and S. M. Peregudova, *Russ. Chem. Rev.*, 1993, **62**, 121 (*Usp. Khim*., 1993, **62**, 135).
66 S. Ketkov, N. Isachenkov, E. Rychagova and W.-B. Tzeng, *Dalton Trans.*, 2014, **43**, 17703.
67 S. Y. Ketkov and H. L. Selzle, *Z. Phys. Chem.*, 2007, **221**, 597.
68 S. N. Pieniazek, F. R. Clemente and K. N. Houk, *Angew. Chem., Int. Ed.*, 2008, **47**, 7746.
69 S. Y. Ketkov, E. A. Rychagova, G. Y. Zhigulin, S. Y. Tzeng and W. B. Tzeng, *High Energy Chem.*, 2020, **54**, 414.
70 H. Braunschweig, M. Fuss, T. Kupfer and K. Radacki, *J. Am. Chem. Soc.*, 2011, **133**, 5780.
71 M. Zlatar, C.-W. Schläpfer, E. P. Fowe and C. A. Daul, *Pure Appl. Chem.*, 2009, **81**, 1397.
72 B. E. Applegate, T. A. Miller and T. A. Barckholtz, *J. Chem. Phys.*, 2001, **114**, 4855.
73 B. E. Applegate, A. J. Bezant and T. A. Miller, *J. Chem. Phys.*, 2001, **114**, 4869.
74 H. Ihee, J. S. Feenstra, J. Cao and A. H. Zewail, *Chem. Phys. Lett.*, 2002, **353**, 325.
75 B. E. Applegate, T. A. Barckholtz and T. A. Miller, *Chem. Soc. Rev.*, 2003, **32**, 38.
76 R. F. W. Bader, *Atoms in Molecules: A Quantum Theory*, Oxford University Press, Oxford, 1990.
77 F. Cortés-Guzmán and R. F. W. Bader, *Coord. Chem. Rev.*, 2005, **249**, 633.
78 D. W. Clark and K. D. Warren, *Inorg. Chim. Acta*, 1977, **24**, 35.
79 D. W. Clack and K. D. Warren, *Struct. Bonding*, 1980, **39**, 1.
80 J. Weber, M. Geoffroy, A. Goursot and E. Penigault, *J. Am. Chem. Soc.*, 1978, **100**, 3995.
81 O. Kostko, B. Bandyopadhyay and M. Ahmed, *Annu. Rev. Phys. Chem.*, 2016, **67**, 19.
82 S. Y. Eom, D. W. Kang and C. H. Kwon, *Phys. Chem. Chem. Phys.*, 2021, **23**, 1414.
83 Y. R. Lee, M. H. Kim and C. H. Kwon, *J. Chem. Phys.*, 2019, **151**, 164305.
84 S. Ghosh, P. Verma, C. J. Cramer, L. Gagliardi and D. G. Truhlar, *Chem. Rev.*, 2018, **118**, 7249.
85 H. Zhao, Y. Pan and K.-C. Lau, *Phys. Chem. Chem. Phys.*, 2023, **25**, 16921.
86 C. J. Stein, V. von Burg and M. Reiher, *J. Chem. Theory Comput.*, 2016, **12**, 3764.
87 M. Feldt and Q. M. Phung, *Eur. J. Inorg. Chem*., 2022, e202200014.
88 H. Neugebauer, H. T. Vuong, J. L. Weber, R. A. Friesner, J. Shee and A. Hansen, *J. Chem. Theory Comput.*, 2023, **19**, 6208.
89 M. Drosou, C. A. Mitsopoulou and D. A. Pantazis, *J. Chem. Theory Comput.*, 2022, **18**, 3538.
90 H. M. Aðalsteinsson and R. Bjornsson, *Phys. Chem. Chem. Phys.*, 2023, **25**, 4570.

Received: 8th February 2024; Com. 24/7390